Available online at www.sciencedirect.com
ScienceDirect
Journal of the European Ceramic Society 31 (2011) 385–389
www.elsevier.com/locate/jeurceramsoc

Influence of glass phase on Al_2O_3 fiber-reinforced Al_2O_3 composites processed by slip casting

Antonio Licciulli [a,*], Vincenzo Contaldi [a], Sanosh Kunjalukkal Padmanabhan [a], Avinash Balakrishnan [b], Cristina Siligardi [c], Daniela Diso [d]

[a] *Department of Engineering for Innovation, University of Salento, 73100 Lecce, Italy*
[b] *Amrita Centre for Nanosciences and Molecular Medicine, Kochi 682041, India*
[c] *Department of Materials and Environmental Engineering, University of Modena and Reggio Emilia, Via Vignolese 905, 41100 Modena, Italy*
[d] *Salentec srl, Via dell'Esercito 8, Cavallino, Lecce, Italy*

Received 24 June 2010; received in revised form 3 October 2010; accepted 11 October 2010
Available online 11 November 2010

Abstract

The present work describes the processing of alumina fiber reinforced alumina ceramic preforms consisting of chopped Al_2O_3 fibers (33 wt%) and Al_2O_3 (67 wt%) fine powders by slip casting. The preforms were pre-sintered in air at 1100 °C for 1 h. A lanthanum based glass was infiltrated into these preforms at 1250 °C for 90 min. Linear shrinkage (%) was studied before and after glass infiltration. Pre-sintered and infiltrated specimens were characterized by scanning electron microscopy, energy dispersive X-ray, X-ray diffraction, porosimetry and flexural strength. The alumina preforms showed a narrow pore size distribution with an average pore size of ∼50 nm. It was observed that introducing Al_2O_3 fibers into Al_2O_3 particulate matrix produced warp free preforms with minor shrinkage during pre-sintering and glass infiltration. It was observed that the infiltration process fills up the pores and considerably improves the strength and reliability of alumina preform.

Keywords: Fiber reinforced ceramic; Glass infiltration; Shrinkage; Strength

1. Introduction

Dental ceramics are commonly used as restorative materials for crowns, bridges, and fixed partial dentures. These ceramics offer higher degrees of esthetics and biocompatibility compare to conventional porcelain ceramics and metal–ceramics systems [1,2]. While processing these ceramics, the sintering stage is very crucial; since energy costs are involved and mechanical properties of these ceramics depend on it. It is well known that the sintering process of the ceramic materials can be improved by using sintering additives [3,4]. Dense ceramic is achievable through glass infiltration process in porous ceramics [5–7]. The glass infiltration technique can improve the mechanical properties of the ceramic by increasing the density and by generation of compressive residual stress on the surface and the blunting of fine surface cracks produced during the sintering and machining process [4,8,9]. The most commonly used technique to obtain a porous ceramic or 'preform' involves pre-sintering, i.e. heating to a low or insufficient sintering temperature. In order to achieve a homogenous infiltration it is important that the preform has skeleton framework with open, continuous porosity and sufficient rigidity, enabling it to take in and withstand the capillary effect of molten glass infiltration [10]. It is been reported [11,12] that preforms consisting of fibers (different than parent matrix) show higher load bearing capacity than those without fibers. This was attributed to the dissipation of the stresses under applied load. In the present study Al_2O_3 fibers were introduced into Al_2O_3-particulate based preform and processed using a simple slip casting technique. The preforms processed showed narrow pore size distribution with an average pore size of 50 nm. These preforms were infiltrated with a state of the art La-based glass and tested for their strength. The preforms were also studied for their % linear shrinkage before and after glass infiltration. An interesting observation of this study was the demonstration of the shrinkage of the alumina preform during glass-infiltration, which was contradictory to the expectations.

* Corresponding author. Tel.: +39 0832 297321.
E-mail address: antonio.licciulli@unile.it (A. Licciulli).

0955-2219/$ – see front matter © 2010 Elsevier Ltd. All rights reserved.
doi:10.1016/j.jeurceramsoc.2010.10.018

Table 1
Composition of La-3 glass used in the present study.

	Composition						
	SiO_2	Al_2O_3	B_2O_3	La_2O_3	CeO_2	CaO	TiO_2
Weight (%)	13.89	12.22	17.89	47.43	2.95	2.88	2.74

2. Materials and methods

Porous Al_2O_3 blocks for glass infiltration were prepared by slip casting. The slurry for slip casting consisted of chopped Al_2O_3 fibers (Saffil, UK, average diameter: 3 μm) (33 wt%), and fine Al_2O_3 powder (67 wt%) (AES-23, Sumitomo chemicals, Japan, average particle size: 1.1 μm) mixed in water. An ionic dispersant (Dolapix CE-64) was added to this slurry. The mixture was ball-milled for 30 min to achieve slurry of pouring consistency. The mixed slurry was poured into a plaster of paris mold and dried for 24 h at room temperature to form rectangular green blocks (50 mm × 80 mm × 10 mm). These blocks were pre-sintered in a muffler furnace at 1100 °C for 1 hr at a ramp rate of 3 °C/min. Pore size distribution (PSD) of the pre-sintered blocks were characterized by mercury porosimetry (Thermo Finnigan, Pascal 140 and 240).

In the present study a lanthanum based glass (La-3) was prepared. The glass was prepared by blending different raw materials (quartz, alumina, boric acid, lantanium oxide, cerium oxide, calcium carbonate and titanium oxide), in a platinum crucible and heated at 1500 °C for 2 h. The composition of the La-3 glass (in wt%) is given in Table 1. The molten mixture was quenched in water at room temperature. The resultant glass was crushed into fine powders (−200 mesh size).

The glass infiltration was done by applying a thin layer of glass powder on the surface of porous Al_2O_3 blocks and sintered at 1250 °C at a ramp rate of 3 °C/min and soaking time of 90 min. This procedure was also repeated for the opposite surface. The extra glass on the surface was removed by precision lapping while maintaining the original block dimension. The length of green blocks, sintered preforms and glass-infiltrated Al_2O_3 was determined by a measuring caliper accurate to 0.01 mm. Linear shrinkage (%) during sintering and glass-infiltration were calculated. The samples were machined into 1.2 mm × 4 mm × 20 mm specimens as per ISO standards (ISO 6872) for three point bend test. The specimens were tested with a universal testing machine (Loyd-LR 5K (USA)), rested on a self-aligning fixture with a span of 16 mm. Tests were conducted at a crosshead speed of 1 mm/min at room temperature.

The uniaxial flexural strength (σ_f) was measured with the three-point bending test and calculated by the following equation:

$$\sigma_f = \frac{3WL}{2bd^2} \quad (1)$$

where W is the breaking load (N); L is the test span (mm), b is the width of the specimen (mm); d is the thickness of the specimen (mm).

The glass infiltrated samples were micro-polished in successive step to 1 μm to obtain a mirror finish. X-ray diffraction (XRD) (Rigaku, Japan) pattern was obtained with Cu Kα radiation (λ = 1.5418 Å) in the step scanning mode recorded in the 2θ range of 20–60°, with a step size of 0.02° and step duration of 0.5 s. The microstructure and phase analysis of the specimen was done using scanning electron microscope (Zeiss-Germany)–energy dispersive X-ray (SEM-EDX) (INCA, Oxford instruments).

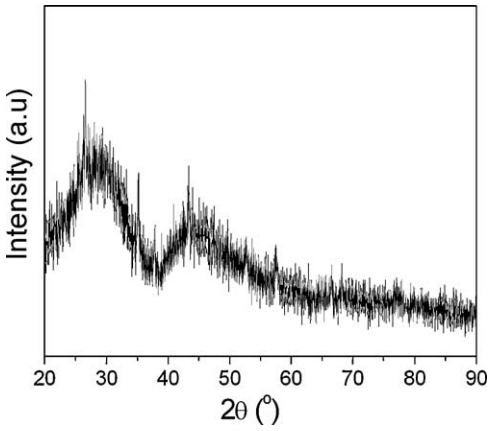

Fig. 1. XRD of La-3 glass.

The fracture strength σ_f data were further analyzed with the conventional ranking method [13] to yield the Weibull parameters, knowledge of which would lead to complete characterization of the statistical properties of the measured σ_f data. This was done by arranging the data in ascending order. The ith result in the set of $n = 15$ data was assigned a cumulative probability of occurrence, P_i, which was calculated with:

$$P_i = \frac{i}{n+1} \quad (2)$$

The measured σ_f and P_i, were then analyzed, by using a simple, least-square regression method, according to the alternative form of the well-known two-parameter Weibull distribution equation:

$$\ln\left[\ln\left(\frac{1}{1-P_i}\right)\right] = m\ln\sigma_f - m\ln\sigma_0 \quad (3)$$

where m and σ_0 are the Weibull modulus and the characteristic strength, respectively.

3. Results

Fig. 1 shows the XRD patterns of La-3 glass which exhibits amorphous behaviour, with no well-defined crystalline peaks.

Fig. 2a shows the SEM image of the mixed powder obtained from the dried slurry. Fig. 2b displays the SEM image of the surface of pre-sintered Al_2O_3 block at 1100 °C for 1 h. The blocks exhibited chalky appearance with chopped Al_2O_3 fibers in the matrix. Fig. 2c shows the pore size distribution (PSD) of the pre-sintered Al_2O_3 block. The PSD curve seemed to be skewed and narrow with pore size centred at ∼50 nm. The total porosity of the pre-sintered blocks was found to be ∼20%.

The linear shrinkage in pre-sintered blocks (measured for five blocks) was found to be 0.049 ± 0.011%. After glass infiltration the linear shrinkage increased to 0.086 ± 0.014%. The shrinkage

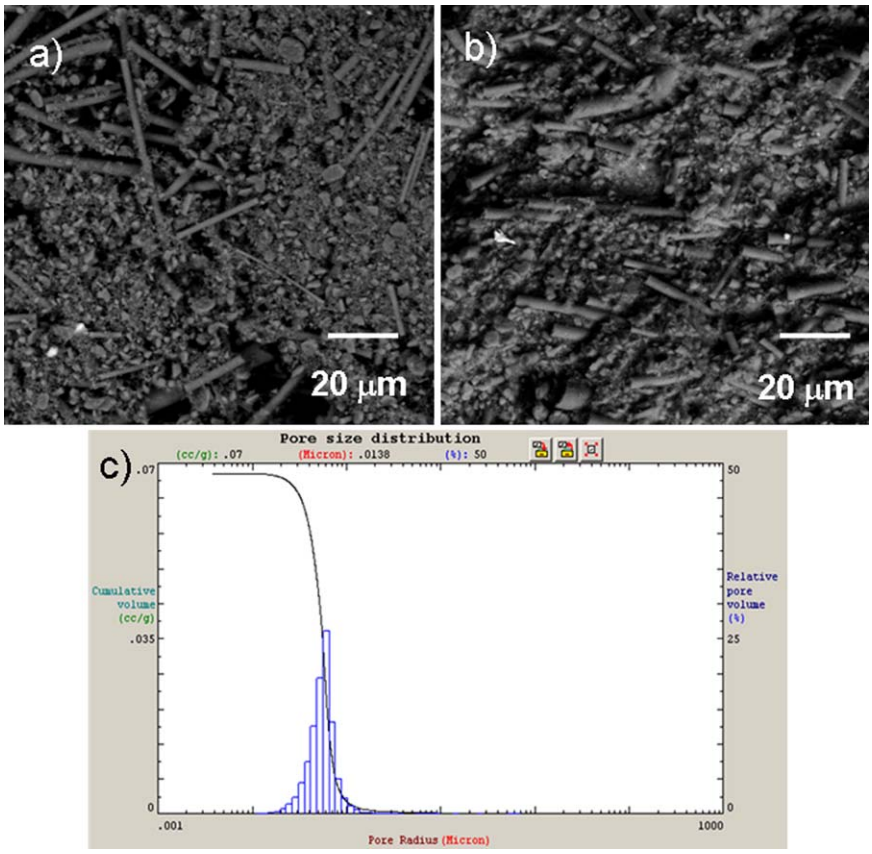

Fig. 2. (a) SEM image of the ball milled powder, (b) SEM image of Al_2O_3 fiber-reinforced Al_2O_3-based ceramic perform; pre-sintered at 1100 °C for 1 h and (c) porosimetry analysis of the perform; pre-sintered at 1100 °C for 1 h.

was found to be uniform in the two axes (i.e. along the length and breadth) with no warping or cracking of the samples. Since the glass was penetrated along the direction of thickness of sample and later lapped for removing extra glass, this axis was not considered for shrinkage measurement.

XRD analysis (Fig. 3) of La-3 infiltrated samples revealed small crystalline peaks of Lanthanum silicate ($La_2Si_2O_7$).

Comparing with standard peaks of alumina (JCPDS file no: 75-0787), no shifts in alumina peaks were observed during glass infiltration. XRD peaks shifts indicating residual compression are reported in other studies [9,14] where low coefficient of thermal expansion (CTE) glass is used for infiltration. However for the La-3 glass composition used in the present study, the CTE measured by dilatometer was found to be $\sim 7.6 \times 10^{-6}/°C$ which was in proximity to alumina ceramics ($8.1 \times 10^{-6}/°C$) [9,13].

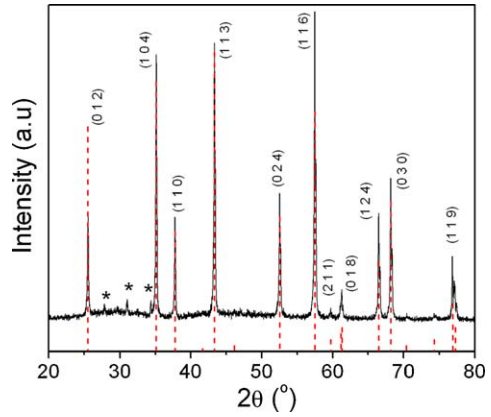

Fig. 3. XRD of glass infiltrated alumina. (*) Shows the presence of $La_2Si_2O_7$ crystalline phases. Dotted lines are the standard peaks for alumina (JCPDS file no: 75-0787).

Fig. 4(a–c) shows the SEM-EDX of the pre-sintered blocks infiltrated with La-3 glass at 1250 °C for 90 min. The EDX analysis confirmed the presence of La-3 glass in the Al_2O_3 matrix (Fig. 4b). The infiltrated La-3 glass (seen in white phases) seems to fill the open pores in the pre-sintered block. The Al_2O_3 grains exhibited both rod and spheroid like grain structure. Some grain pull outs were observed during the polishing of the sample.

Fig. 5 compares the flexural strength of glass infiltrated samples with pre-sintered blocks obtained in this work. It was seen that the glass infiltrated Al_2O_3 exhibited strength $\sigma_0 = 545$ MPa, while pre-sintered samples showed strength $\sigma_0 = 33$ MPa. However, there was a significant increase in Weibull modulus, i.e. decrease in scattering of the data for glass infiltrated Al_2O_3.

4. Discussion

Glass infiltration has become one of the promising methods towards the production of high strength ceramic matrix composites. Inorder to achieve a homogenous infiltration, it is important

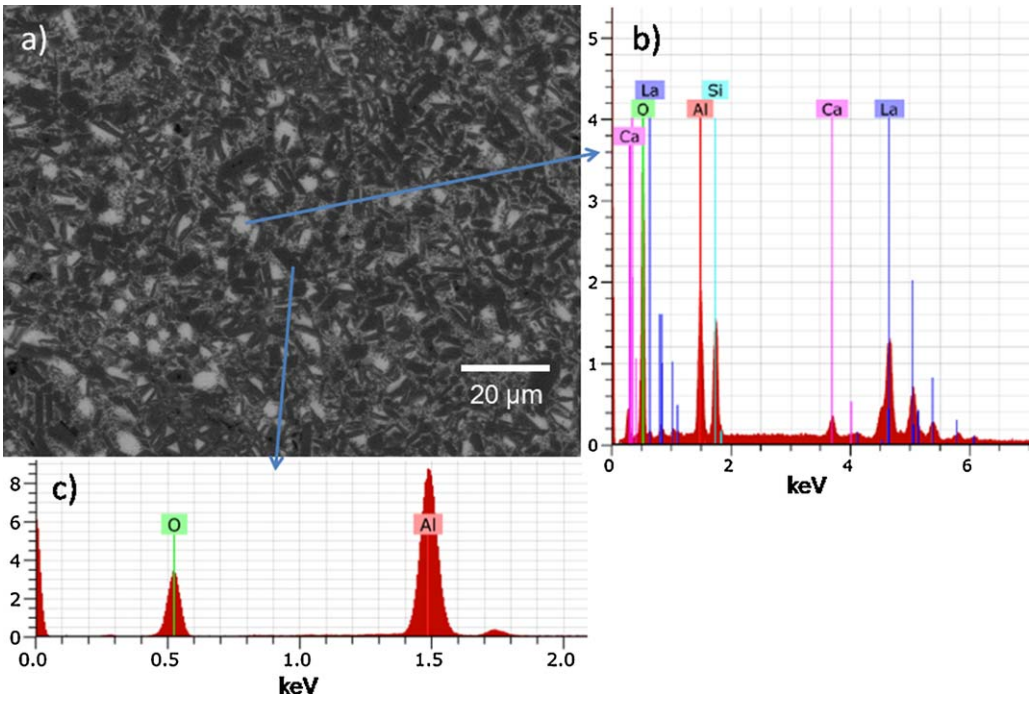

Fig. 4. (a) SEM image of glass infiltrated alumina, (b) EDX analysis of the glass (white) phase and (c) alumina grain (grey).

that a mechanically stable, self sustaining porous preform of ceramic with a reinforcing phase like fibers or particles is prepared. In case of Al_2O_3, to obtain good strength and stable pre-form, generally it is pre-sintered in the temperature range from 1050 to 1200 °C. It is reported that pre-sintering Al_2O_3 powder compacts with bimodal particle size distribution is quite beneficial. The large particles are bonded to each other by surface diffusion and fusion of fine particles located in the contact area between large ones. This means that fine particles get partially sintered while large ones may not [14–19]. Such pre-sintering leads to porous and rigid Al_2O_3 ceramic. In the present study, this kind of particle sintering was undertaken by introducing Al_2O_3 fibers into the Al_2O_3 powder, so that framework with open, continuous porosity and certain rigidity is obtained. The sintering was evident by the shrinkage ($0.049 \pm 0.011\%$) of green blocks during the heating at 1100 °C. This shrinkage was found be

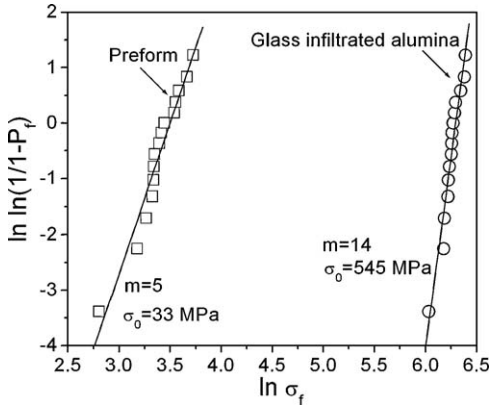

Fig. 5. Weibull plot of preform and glass infiltrated alumina.

~4 times less that in-ceram alumina samples which reportedly showed $0.21\% \pm 0.10\%$ under similar pre-sintering conditions [20]. Further no warping or cracking of the pre-sintered and glass infiltrated blocks indicated that dispersion of the fibers in the Al_2O_3 matrix (Fig. 2b) not only helps in the formation of uniform pore size (narrowly distributed pore size, Fig. 2c) but also seem to reduce the stress concentrations. It is obvious that shrinkage of these preforms would increase at higher sintering temperatures and the longer sintering times. It been reported that higher sintering temperatures for Al_2O_3 compacts yielded higher elastic moduli of preforms [14]. This means that the pre-sintered porous Al_2O_3 could attain the needed mechanical properties for machining without damage before glass infiltration and resist to deformation during capillary infiltration of molten glass. In the present study, it was found that the Al_2O_3 blocks with fibers, pre-sintered at temperature 1100 °C for 1 h has sufficient tolerance to glass infiltration without any structural breakdown.

Interestingly, glass infiltrated Al_2O_3 showed further shrinkage $0.086 \pm 0.014\%$, i.e. ~ 43% more shrinkage after pre-sintering. Shrinkage of preforms during glass infiltration has also been reported by other researchers. For instance, Kim et al. reported 0.34–0.05% [21] linear shrinkage in glass infiltrated alumina preforms that was processed by slip-casting. The shrinkage was mainly attributed to the liquid phase sintering of alumina taking place during the glass-infiltration process. This sintering could affect glass composition and crystallization behaviour during the infiltration. Some glass compositions crystallize easily during infiltration (i.e. become highly viscous), while other compositions do not. Rapid crystallization can reduce the viscosity of the molten glass and inhibit further infiltration. This possibly can have adverse effect on the densification and mechanical

properties of the glass infiltrated samples. For the present La-3 glass composition, it was seen that after two thermal cycles for glass infiltration, did not prevent glass phase from being dispersed in the Al_2O_3 matrix (Fig. 4) and resulted in a marked increase in strength values of pre-sintered Al_2O_3 preforms combined with a significant increase in the Weibull modulus (Fig. 5). The increase in strength and Weibull modulus may be associated to surface defect healing by molten glass during infiltration. Thus results indicate that the La-3 glass composition was suitable for infiltration with a positive effect on the strength properties.

In the present study, glass infiltrated samples show ∼30% higher strength (525 MPa) compare to sintered alumina (∼380 MPa) having >99% relative density [13,22]. There are different strength values reported for alumina infiltrated with different glasses [23–29]. For instance, Lou et al. [28] in their work used MgO modified glass to infiltrate partially sintered alumina and attained strength of 432 MPa. While, Chu et al. [29] in his work infiltrated sintered alumina using magnesium aluminum silicate glass to attain strength of 625 MPa. This means that based on the required application, different glasses and infiltration processes could be designed to attain different properties for alumina. However, the present technique could be adapted to various types of dental ceramic materials such as crowns, bridges, and laminate veneers because of its simple processing, reproducibility and good mechanical properties.

5. Conclusions

In the present study, slip casting technique was used to develop a near net shaped Al_2O_3 fiber-reinforced Al_2O_3-based ceramic preforms. The preforms developed by this method showed narrow pore size distribution and very less shrinkage with no warping or cracking after pre-sintering. Pre-forms were rigid enough to withstand the glass infiltration. Minimal shrinkage was observed during the glass infiltration of these Al_2O_3 preforms. The glass infiltrated samples showed high strength values combined with a significant increase in the Weibull modulus. However, further studies are needed to understand the sintering mechanisms involving the glass phase in these Al_2O_3–fiber/Al_2O_3 composite.

References

1. Raigrodski AJ, Chiche GJ. The safety and efficacy of anterior ceramics fixed partial denture: a review of the literature. *J Prosthet Dent* 2001;**86**:520–5.
2. Little DA, Crocker JJ. Clinical use of new metal-free restorative technology: case reports. *Dent Today* 2002;**21**:68–72.
3. Acchar W, Ramalho EG, Hotza D, Segadaes AM. Using granite rejects to aid densification and improve mechanical properties of alumina bodies. *J Mater Sci* 2005;**40**:3905–9.
4. Guazzato M, Albakry M, Quach L, Swain MV. Influence of surface and heat treatments on the flexural strength of a glass-infiltrated alumina/zirconia-reinforced dental ceramic. *Dent Mater* 2005;**21**:454–63.
5. Guazzato M, Albakry M, Ringer SP. Strength, fracture toughness and microstructure of a selection of al-ceramic materials. Part I. Pressable and alumina glass-infiltrated ceramics. *Dent Mater* 2004;**20**: 441–8.
6. Sheng XJ, Xu H, Jin ZH, Wang YL. Preparation of glass-infiltrated 3Y-TZP/Al_2O_3/glass composites. *Mater Lett* 2004;**58**:1750–3.
7. Peitl O, Orefice RL, Hench LL, Brennan AB. Effect of the crystallization of bioactive glass reinforcing agents on the mechanical properties of polymer composites. *Mater Sci Eng A* 2004;**372**:245–51.
8. Wolf WD, Vaidya KJ, Francis LF. Mechanical properties and failure analysis of alumina–glass dental composites. *J Am Ceram Soc* 1996;**79**:1769–76.
9. Balakrishnan A, Panigrahi BB, Chu MC, Kim TN, Cho SJ. Microindentation fracture behaviour of surface modified alumina ceramic using glass infiltration. *J Mater Proc Technol* 2009;**209**:1783–8.
10. Hang W, Yunmao L, Yonglie C, Xing L. Shrinkage and strength characterization of an alumina–glass interpenetrating phase composite for dental use. *Dent Mater* 2007;**23**:1108–13.
11. Tanimoto Y, Nishiwaki T, Nishiyama N, Nemoto K, Maekawa Z. A simplified numerical simulation method of bending properties for glass fiber cloth reinforced denture base resin. *Dent Mater J* 2002;**21**:105–17.
12. Michaud V, Mortensen A. Infiltration processing of fibre reinforced composites: governing phenomena. *Compos Part A* 2001;**8**:981–96.
13. Schneider SJ. *Engineered materials handbook, ceramics and glasses*, vol. 4. USA: ASM International; 1991.
14. Colloidal and thermal processing variables for alumina–glass dental composites.Wolf WD, Francis LF, Fischman G, Clare A, Hench L, editors. *Bioceramics: Materials and Applications*, vol. 48. Ceram Trans; 1995. p. 261–8.
15. Shiau FS, Fang TT, Leu TH. Effect of particle-size distribution on the microstructural evolution in the intermediate stage of sintering. *J Am Ceram Soc* 1996;**80**:286–90.
16. Franklin SA, Rand B. Partial sintering in porous alumina refractories: effect of size distribution on microstructure and elastic modulus. *Br Ceram Trans* 1996;**95**:93–8.
17. O'Hara MJ, Cutler IB. Sintering kinetics of binary mixtures of alumina powders. *Br Ceram Proc* 1969;**2**:145–54.
18. Smith JP, Messing GL. Sintering of bimodally distributed alumina powders. *J Am Ceram Soc* 1984;**67**(4):238–42.
19. Taruta S, Itou Y, Takusagawa N. Influence of aluminum titanate formation on sintering of bimodal size-distributed alumina powder mixtures. *J Am Ceram Soc* 1997;**80**:551–6.
20. Campbell SD, Pelletier LB, Pober RL, Giordano RA. Dimensional and formation analysis of a restorative ceramic and how it works. *J Prosthet Dent* 1995;**74**:332–40.
21. Kim DJ, Lee MH, Kim CE. Mechanical properties of tape-cast alumina–glass dental composites. *J Am Ceram Soc* 1999;**82**:3167–72.
22. Munro RG. Evaluated material properties for a sintered alpha-Al_2O_3. *J Am Ceram Soc* 1997;**80**:1919–28.
23. Della-Bona A, Mecholsky Jr JJ, Barrett AA, Griggs JA. Characterization of glass-infiltrated alumina-based ceramics. *Dent Mater* 2008;**24**:1568–74.
24. Massimiliano G, Mohammad A, Simon PR, Michael VS. Strength, fracture toughness and microstructure of a selection of all-ceramic materials. Part I. Pressable and alumina glass-infiltrated ceramics. *Dent Mater* 2004;**20**:441–8.
25. Massimiliano G, Mohammad A, Linda Q, Michael VS. Influence of grinding, sandblasting, polishing and heat treatment on the flexural strength of a glass-infiltrated alumina-reinforced dental ceramic. *Biomaterials* 2004;**25**:2153–60.
26. Salazar Marocho SM, Studart A, Bottino MA, Della-Bona A. Strength, subcritical crack growth and lifetime of glass-infiltrated alumina-based ceramics. *Dent Mater* 2009;**25**:e44.
27. Fischer H, Weiß R, Telle R. Crack healing in alumina bioceramics. *Dent Mater* 2008;**24**:328–32.
28. Lou XP, Tian JM, Zhang YL, Ling W. Strength and fracture toughness of MgO-modified glass infiltrated alumina for CAD/CAM. *Dent Mater* 2002;**18**:216–20.
29. Chu MC, Panigrahi BB, Balakrishnan A, Cho SJ, Yoon KJ, Kim TN, et al. Strengthening of alumina by a low thermal expansion glass at surface. *Mater Sci Eng A* 2007;**452–453**:110–5.